ESRF BAG report MX2443

Title of BAG	The Iberian cryo-EM Community		
Main Proposer	Jaime Martín-Benito Romero. National Center for Biotechnology. Spanish Research Council. jmartinb@cnb.csic.es		
BAG Members (PIs/Affiliation)	Ana Luisa Carvalho, FCT; Alberto Marina Moreno, IBV; Margarida Archer, ITQB; Beatriz Herguedas Francés, BIFI; Carmen San Martín, CNB; Clara Marco, IBV; Célia Romão, ITQB; Cristina Vega, CIB; Daniel Lietha, CIB; Daniel Luque, ISCII; Ernesto Arias palomo, CIB; Elin Moe, ITQB; Ignasi Fita, IBMB; Israel Sánchez, IBMB; Iban Ubarretxena, EHU; Jose Maria Casasnovas, CNB; Javier Garcia-nafria, BIFI; Jose Luís Llacer Guerri, IBV; Jaime Martin-Benito Romero, CNB; Jose María Valpuesta, CNB; Jose Castón, CNB; Manuel Palacín, IRB; Pedro Matias, ITQB; Miquel Coll, IRB; María Joao Romao, FCT; Marcelo Guerin, BIOGUNE; Nuria Verdaguer,IBMB; Oscar Llorca, CNIO; Patricia Casino Ferrando, UV; Pedro Pereira, IBMC; Rafael Fernandez-Leiro, CNIO; Santiago Ramon-Maiques, IBV; Sean Connell, BIOGUNE; Sandra Ribeiro, IBMC; Teresa Santos-Silva, FCT; Armando Albert, IQFR; Juan Hermoso, IQFR; Julia Sanz Aparicio, IQFR; María José Sanchez Barrena, IQFR; Jerónimo Bravo, IBV.		
Proposal Reference Number	MX2443	**Date of Report**	September 5th 2023
Sessions Reported			

Number of EMDB/PDB submissions since last report	New EMDB deposited: 20 EMDB IDs: EMD-14313, EMD-14314, EMD-14315, EMD-12747, EMD-12748, EMD-12750, EMD-12751, EMD-12752, EMD-12753, EMD-12754, EMD-12755, EMD-12941, EMD-12942, EMD-12943, EMD-12944, EMD-13482, EMD-14729, EMD-14706, EMD-14727, EMD-14736. New PDB deposited: 16 PDB IDs: 7R4R, 7R4Q, 7RAI, 7O7L, 7O7M, 7O7N, 7O7O, 7O7P, 7O7Q, 7O7R, 7O7S, 6TAV, 4ACQ, 6ZN2, 7PKR, 7ZHS.
Number of publications since last report	5

References of publications using cryoEM data obtained in the ESRF

1.
Casasnovas JM, Margolles Y, Noriega MA, Guzmán M, Arranz R, Melero R, Casanova M, Corbera JA, Jiménez-de-Oya N, Gastaminza P, Garaigorta U, Saiz JC, Martín-Acebes MÁ, Fernández LÁ. Nanobodies Protecting from Lethal SARS-CoV-2 Infection Target Receptor Binding Epitopes Preserved in Virus Variants Other Than Omicron. Front Immunol. 2022 Apr 25; 13:863831. doi: 10.3389/fimmu.2022.863831. eCollection 2022. PMID: 35547740.
EMDB IDs: EMD-14313, EMD-14314, EMD-14315.
PDB IDs: 7R4R, 7R4Q, 7RAI.

2.
Luque D, Goulas T, Mata CP, Mendes SR, Gomis-Rüth FX, **Castón JR**. Cryo-EM structures shows mechanisitics basis of pan-peptidase inhibition by human α2-macroglobulin. Proc Natl Acad Sci U S A. 2022 May 10;119(19):e2200102119. doi: 10.1073/pnas.2200102119. Epub 2022 May 2. PMID: 35500114.
EMDB IDs: EMD-12747, EMD-12748, EMD-12750, EMD-12751, EMD-12752, EMD-12753, EMD-12754, EMD-12755, EMD-12941, EMD-12942, EMD-12943, EMD-12944.
PDB IDs: 7O7L, 7O7M, 7O7N, 7O7O, 7O7P, 7O7Q, 7O7R, 7O7S, 6TAV, 4ACQ

3.
Bueno-Carrasco MT, Cuéllar J, Flydal MI, Santiago C, Kråkenes TA, Kleppe R, López-Blanco JR, Marcilla M, Teigen K, Alvira S, Chacón P, Martinez A, **Valpuesta JM**. Structural mechanism for tyrosine hydroxylase inhibition by dopamine and reactivation by Ser40 phosphorylation. Nat Commun. 2022 Jan 10;13(1):74. doi: 10.1038/s41467-021-27657-y. PMID: 35013193.
EMDB IDs: EMD-13442.
PDB IDs: 6ZN2.

EMD-11624, EMD-11467, EMD-11309, EMD-11587

4.
Velasco-Carneros L, Cuéllar J, Dublang L, Santiago C, Maréchal JD, **Martín-Benito J**, Maestro M, Fernández-Higuero JA, Orozco N, Moro F, **Valpuesta JM**, Muga A. "The self-association equilibrium of class A J-domain proteins DNAJA2 regulates its interaction with unfolded substrate proteins and with Hsc70. 2023. Nat. Commun (in the press)

5.
Guerra P, González-Alamos M, Llauró A, Casañas A, Querol-Audí J, de Pablo PJ, **Verdaguer N**. Symmetry disruption commits vault particles to disassembly. Sci Adv. 2022 Feb 11;8(6):eabj7795. doi: 10.1126/sciadv.abj7795. Epub 2022 Feb 9. PMID: 35138889.
EMDB IDs: EMD-13478, EMD-13483, EMD-13482.
PDB IDs: 7PKR

(BAG members are shown in bold type)

Beam-time reports

RNA polymerase of the infectious bursal disease virus (JR Castón/Jose Fdez-Palacios)

Session	Date	Micrographs	Ptcls	Fractions	Å/px	Images/hole
MX2443	25-27/11/2022	21341		60	0.84	
MX2443	22–24/03/2023					

On the 25th of November of 2023 to the 27th, we utilized the cryo-electron microscopy services at the European Synchrotron Radiation Facility (ESRF) to examine our protein of interest (the RNA polymerase of the infectious bursal disease virus).

Our local contact at the facility was Traore Daouda. The facility provided excellent services, meeting all of our needs in a timely and professional manner. The facility staff were knowledgeable and helpful throughout the entire process. Communication with our local contact was fluent. We held a brief meeting to discuss the details of the acquisition and he frequently reported the status of the acquisition during the session. He also provided us with clear instructions about how to transfer the data to our machines. Finally, we found the data processing services at the facility very convenient. Our samples also returned correctly to our laboratory.

As for the details regarding the data acquisition and processing, our sample was vitrified in UltrAufoil R0.6/1 grids and 21341 movies were recorded at a pixel size of 0.84. After motion correction and CTF estimation, micrographs (16195) that displayed a better than 3.5 A resolution were selected (**Figure 1**). Due to the high number of particles in each micrograph, they were divided into 5 subsets of 3239 micrographs.

From 150 micrographs, 252,270 particles were reference-free picked using the general model from crYOLO, extracted with a box size of 256 px and binned to 64 px. After two rounds of 2D classification, 67,258 particles were selected and subjected to ab initio reconstruction in CryoSPARC. The best model was refined to 3.4 A using the non uniform refinement job from CryoSPARC with the unbinned particles.

A set of 100 projections was generated from the resulting model (low-pass filtered to 20 A), which were used for particle picking with Gautomatch. Approximately, 6.1 million particles were picked for each subset, which were processed independently. Resulting picks were extracted using a box of 256 px, binned to 64 px and subjected to two rounds of 2D classification using CryoSPARC (**Figure 2**). Resulting particles (1.9 million) were then subjected to one round of ab initio reconstruction and heterogeneous refinement using 6 volumes. Particles that belonged to the best two classes were selected (1.1 million) and used for a non uniform refinement job using the best ab initio model as reference. A map of 2.7 A resolution was obtained.

The same processing pipeline was applied to another subset of 3239 micrographs. Particles resulting from the heterogeneus refinement job were merged with the ones

obtained from the previous subset (2.2 million total) and used for a non uniform refinement job. However, the resulting map stayed at 2.7 A resolution (**Figure 3)**. Efforts to improve these maps are still ongoing.

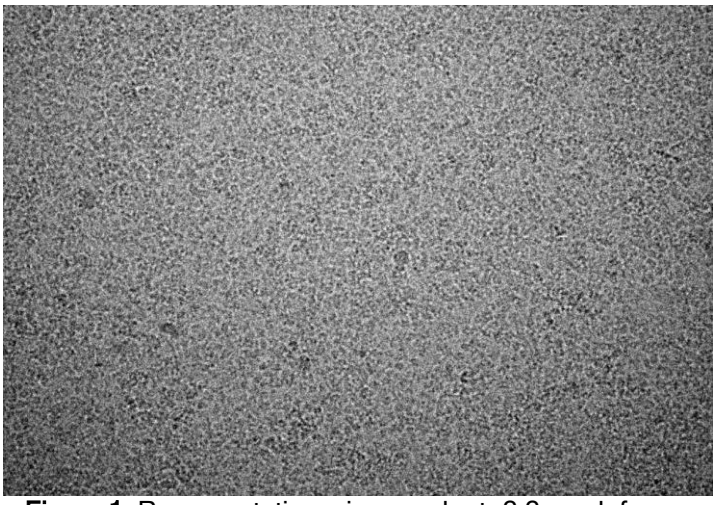

Figure 1. Representative micrograph at -2.2 çm defocus.

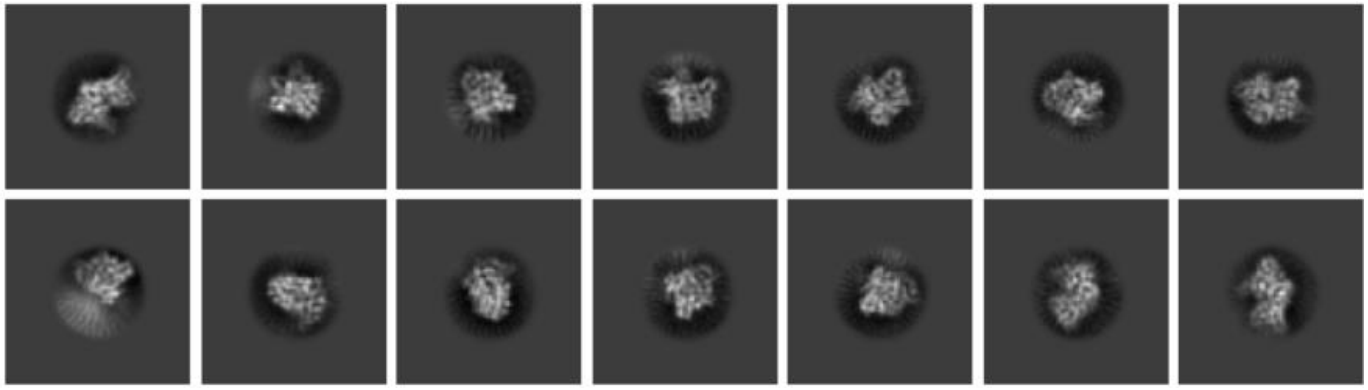

Figure 2. Example of 2D averages obtained from the second round of 2D classification in CryoSPARC.

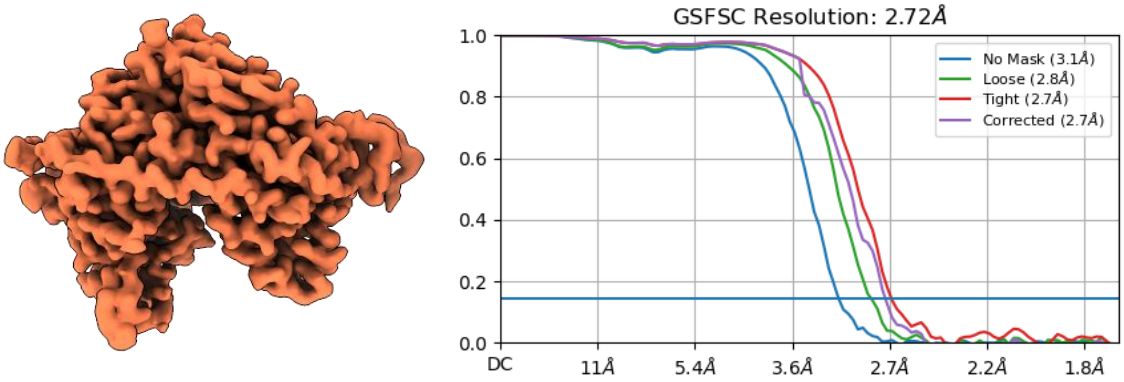

Figure 3. Resulting model and FSC curve from the non-uniform refinement job.

MX2446 – Structure of AMPA receptor in the open conformation (Beatriz Herguedas-Francés)

Session	Date	Micrographs	Ptcls	Fractions	Å/px	Images/hole
MX2443	19-21/09/2022					
MX2443	3-5/07/2023					

In the last year we collected data twice (CM01 19/09/22 and CM01 03/07/23). Our aim was to trap specific AMPA receptor complexes in open conformations. In the first session, we obtained good quality 2Ds but most of the receptor was in a desensitized conformation (2D averages, panel A). Session 2 resulted in excellent quality data (2D averages, panel B), with a preliminary map at 3 Å resolution and the receptor trapped in an open conformation (panel C)

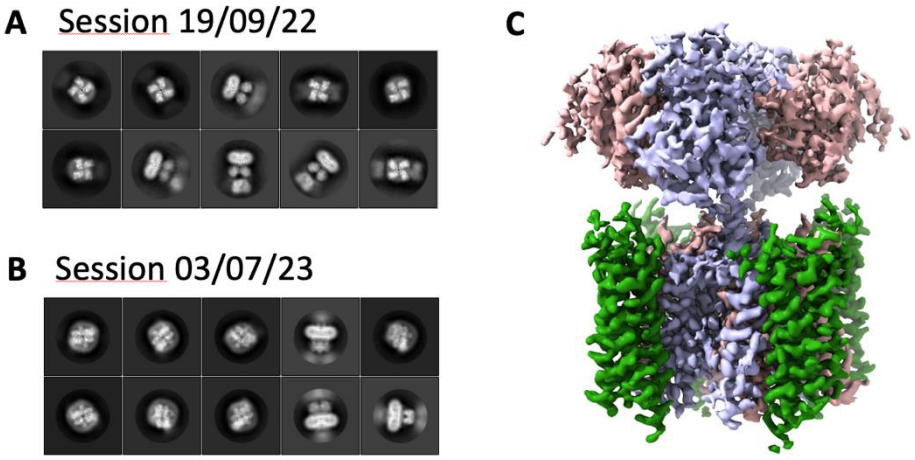

MX2443 - Structure the marine giant virus PkV-RF02 (Carmen San Martín/Sara Otaegi)

Session	Date	Micrographs	Ptcls	Fractions	Å/px	Images/hole
MX2443	20-22/06/2023 17-19/4/2023	16171		24	1.35	1

We collected a dataset of 16171 micrographs of a giant virus around 180 nm in diameter. It was the first cryo-data collection of this specimen.We encountered a problem with the EPU software at data-collection: the software failed in the identification of holes in the Quantifoil film, with a large number of positions placed on the carbon instead. We did trials with different hole patterns size (R1.2/1.3 and R0.6/1) and the problem persisted in all of them. We attributed the problem to the sample characteristics: dark electrodense thick viral particles distributed in the holes as well as in the carbon, producing similar electrodensity on the hole and carbon film. Additionally, as EPU was not recognizing the physical holes well, the threshold for empty/full ice holes didn´t work as well. An attempt to use SerialEM instead of EPU did not improve the situation. Nevertheless, we managed to collect over 16000 movies, although some hundreds were taken on the carbon (Fig. 1A) and some other hundreds without sample. We thank Gregory Effantin for his help with these complicated grids.

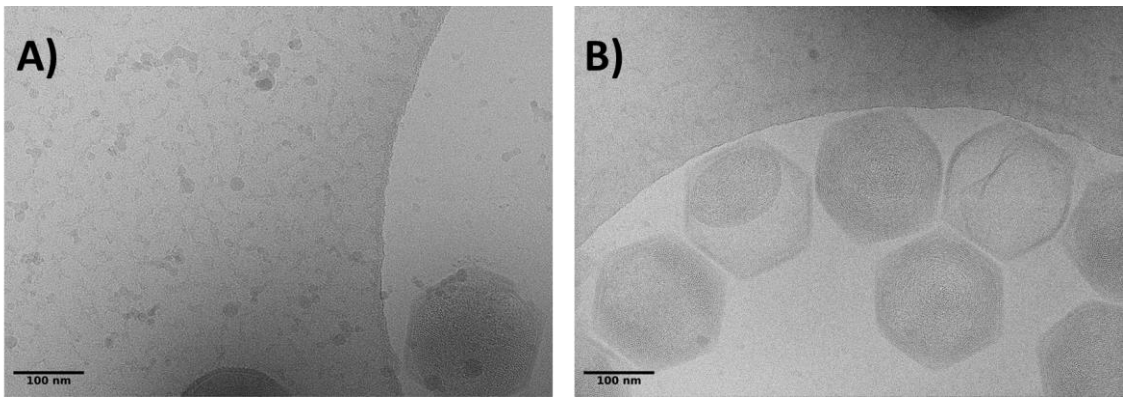

Figure 1. (A) Micrograph taken on the carbon. (B) Representative good micrograph showing heterogeny in particle conformation: F (full particles or genome containing particles), E (empty particles), P (partially filled particles).

For computational analyses, we are using Scipion v3.2.11 to easily combine different software suites in the analysis workflows of cryo-EM data. Movie frames, 24 frames for each movie, were aligned using MotionCor2. The contrast transfer function (CTF) of the micrographs was estimated using CTFFIND4. Based on best defocus values and resolution (rejected the micrographs with around 1.1 defocus ratio and >7 resolution value), 16045 movies were considered to be of good quality.

At present, particles are being picked manually using XMIPP, as autopicking by either XMIPP or GAUTOMATCH produced suboptimal results. In the movies collected, we can observe viral particles in different states of assembly/disassembly: full (genome-containing), empty, and partially filled particles (Fig. 1B). Due to the large particle size, on average we expect to have 1 usable particle per micrograph, even after using a moderate magnification (1.35 Å/px).

With this data collection, we hope to have enough particles to obtain at least a medium resolution first 3D map of the virus, to determine whether on the whole the capsid is icosahedrally ordered, determine its triangulation number, and start modelling the major capsid protein. Unused grids were stored at ESRF (Cane K5, puck 2, name of the puck: ESRF-03, positions 3 and 4) for future, additional data collection.

MX2443 - Structure of a SARS-CoV-2 spike bound to a neutralizing nanobody (José María Casasnovas)

Session	Date	Micrographs	Ptcls	Fractions	Å/px	Images/hole
MX2443	31/05/2023-2/06/2023					

The structures obtained with the data acquired in these sessions were published in the reference:
Casasnovas JM, Margolles Y, Noriega MA, Guzmán M, Arranz R, Melero R, Casanova M, Corbera JA, Jiménez-de-Oya N, Gastaminza P, Garaigorta U, Saiz JC, Martín-Acebes MÁ, Fernández LÁ. Nanobodies Protecting from Lethal SARS-CoV-2 Infection Target Receptor Binding Epitopes Preserved in Virus Variants Other Than Omicron. Front Immunol. 2022 Apr 25; 13:863831. doi: 10.3389/fimmu.2022.863831. eCollection 2022. PMID: 35547740.
Deposit numbers: EMD-14313, EMD-14314, EMD-14315 and PDB IDs: 7R4R, 7R4Q, 7RAI.

Ni-NTA affinity purified S with 6xHis-tag was mixed with the Nb (1:1.5 molar ratio of S monomer:Nb) during 30 min at 10°C, and the S-Nb complex purified by size exclusion chromatography in a Superose 6 (16/60) column with 20 mM Tris-buffer and 200 mM NaCl, pH 7.7. The sample was concentrated to 1mg/ml and applied to glow-discharged holey carbon grids (Quantifoil, Au 300 mesh, R 0.6/1). The grids were blotted and then plunged into liquid ethane using a FEI Vitrobot Mark IV at 4°C. Data were chequed at a FEI Talos Arctica electron microscope operated at 200 kV and equipped with a Falcon III electron detector at the Centro Nacional de Bitecnología (CSIC). Selected grids were sent to Grenoble and a dataset was collected in a Titan Krios instrument at the ESRF CM01 line. At the Talos Arctica, the images were recorded at a defocus range of -1 µm to -2.5 µm with a pixel size of 0.855 Å; exposure time was 40 s, with a total exposure dose of 32 e/Å2 over 60 frames. At the Titan Krios, a super resolution acquisition mode was used with a 105k magnification and a pixel size of 0.84 Å, with a defocus range of -1.0 to -2.4 um in 0.2 um step; the exposure time was of 1.8 s, with a total exposure dose of 39.0 e/Å2 (15.3 e/pixel/s) over 40 frames.

Particle reconstructions were carried out throughout INSTRUCT projects in the Electron Microscopy Image Processing, I2PC, Madrid, which resulted in EM maps of the trimeric S with the bound Nbs. We used Scipion 2.0 (53) in order to easily combine different software suites in the analysis workflows of CryoEM data: Movie frames were aligned using MotionCor2; the contrast transfer function (CTF) of the micrographs was estimated using CTFFIND4; particles were automatically selected from the micrographs using autopicking from Gautomatch. Evaluation of the quality of particles and selection after 2D classifications, the initial volume for 3D image processing, the 3D-classification and the final refinement were calculated using cryoSparc, whereas the sharpening was estimated by DeepEMhancer.

Model building for the S-Nb complexes was performed with a S protein structure (PDB 6ZXN) and Nb models, which were prepared with the program Modeller based on the 1ZV5 (1.10), 3TPK (1.29) and 6DBA (2.15) structures. The S structure and the Nb models were fitted into the EM map with the chimera and coot programs. Subsequently, the structures were subjected to real-space refinement in PHENIX (54), which included cycles of rigid body, global and adp minimization. NCS was applied among the S domains, but excluding the RBDs. Nb-RBD binding interfaces were determined with the PISA server, and main figures of the structures were prepared with pymol (pymol.org). The EM maps and the refined structures have been deposited in the PDB with accession codes 7R4R, 7R4Q and 7R4I for the S-1.10, S-1.29 and S-2.15, respectively.

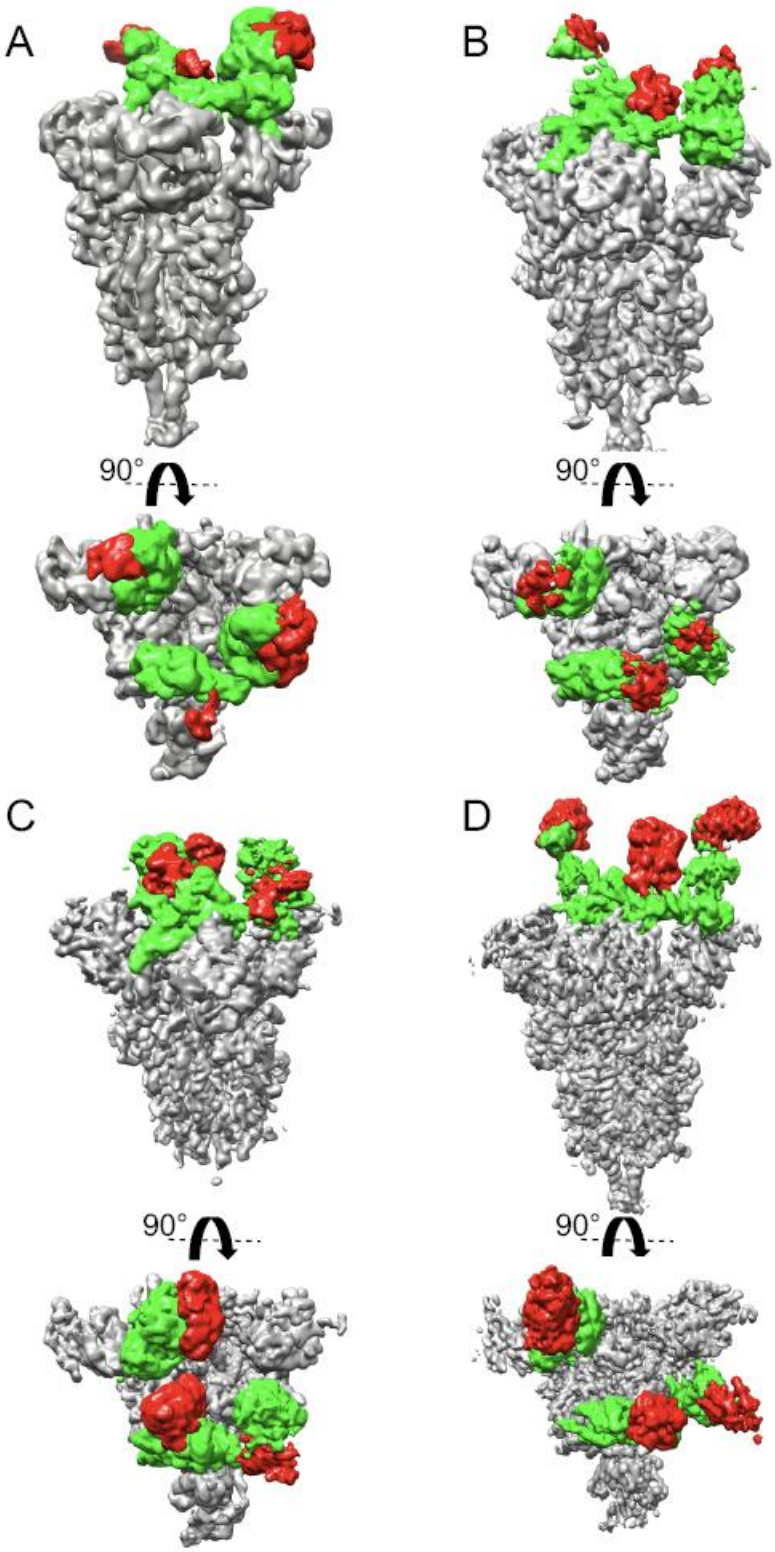

Cryo-EM structures of S-Nb complexes. Surface representations of the maps generated by the reconstruction of the trimeric S with bound 1.10 (A), 1.26 (B), 1.29 (C) or 2.15 (D) Nbs. Map regions corresponding to the Nbs are shown in red, the RBDs in green and the rest of the S in grey.

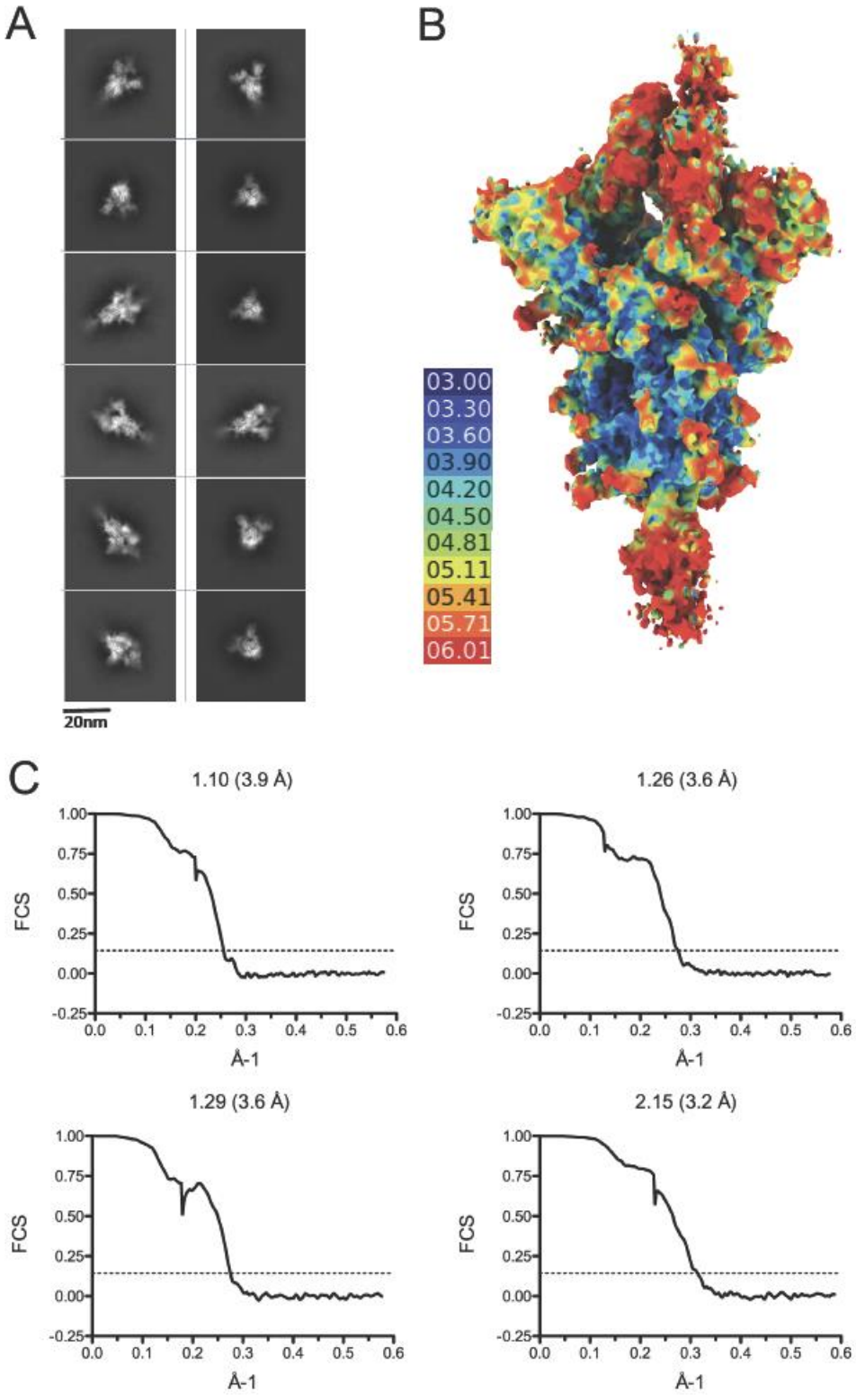

Cryo-EM data processing and S-Nb particle reconstruction. A. Representative 2D average classes. B. S-2.15 complex reconstruction and local map resolution. C. Fourier Shell correlation (FSC) in the S-Nb particle reconstructions. FSC versus resolution (1/Å), and resolution determination at the 0.143 value for the reconstructions of the S with bound 1.10, 1.26, 1.29 or 2.15 Nbs.

MX2443 - Structure of tyrosine hydroxylase deletion mutant (José María Valpuesta)

Session	Date	Micrographs	Ptcls	Fractions	Å/px	Images/hole
MX2443	28-30/11/2022 6-8/02/2023	13213		40	1.07	2

The structure obtained with the data acquired in these sessions were published in the reference:
Bueno-Carrasco MT, Cuéllar J, Flydal MI, Santiago C, Kråkenes TA, Kleppe R, López-Blanco JR, Marcilla M, Teigen K, Alvira S, Chacón P, Martinez A, Valpuesta JM. Structural mechanism for tyrosine hydroxylase inhibition by dopamine and reactivation by Ser40 phosphorylation. Nat. Commun. 2022 Jan 10;13(1):74. doi: 10.1038/s41467-021-27657-y. PMID: 35013193.
EMDB IDs: EMD-13442.
PDB IDs: 6ZN2.

Data acquisitions for THNΔ35(DA) and THS40p were performed at the Diamond Light Source (DLS) electron Bio-Imaging Centre (eBIC) using a Titan Krios electron microscope operated at 300 kV, equipped with a Gatan Quantum K3 detector operated in counting mode with 0.5X-binning (super-resolution mode). A total of 9241 and 13213 movies were acquired for THΔ35(DA) and THS40p respectively, at a nominal magnification of 81,000× with a defocus range of −1.6 to −3.4 µm. Movies were fractionated to 40 frames with a total exposure of 2 s for both samples. The electron dose was 30 e−/Å2 (Supplementary Table 6). Motion-corrected movies were extracted and binned 2 to the physical pixel size of 1.07 Å/pixel.

Image processing of THΔ35(DA) samples was performed following a similar workflow. All programs used to obtain the different 3D models are implemented in the Scipion 2.0 software platform. First, the beam-induced motion of the movies was corrected using the MotionCorr2 software. After movies alignment, the contrast transfer function (CTF) was calculated and corrected by Gctf. Particles were automatically picked with Xmipp3 -auto-picking software. To save computational time during the first processing steps and to increase the signal to noise ratio, particles were downsampled by a factor of 4, and extracted with Xmipp3 – extract particle. The extracted particles were subjected to a first 2D classification using Relion 2.0 and the best classes were subjected to several further rounds of 2D classification, allowing a much better detection of bad particles such as aggregates or particles that were very close to each other.

and THS40p, image processing was performed following similar steps and using Relion-377 and cryoSPARC78. The 3D reconstruction process was carried out with D2 symmetry imposition. After several rounds of 2D and 3D classification, 152,128 and 148,453 particles were re-extracted at the original pixel size and used to generate the final 3D maps at 4.6 and 4.5 Å resolution, respectively

For 3D reconstruction, different de novo initial models were obtained using both EMAN272 and RANSAC73. Another initial model was obtained by low resolution (60 Å) filtering of the atomic structure of the CD of the human TH (PDB 2XSN). The first rounds of 3D classification were performed using Relion 2.0 without any symmetry imposition and using the different initial models. No significant differences were found among the best class obtained from the low-pass filtered atomic structure and the de novo initial model. Particles belonging to that class were subjected to refinement using Relion 2.0– 3D auto-refine software. Since clear

symmetric features were observed in this class, we sought to determine whether C2 or D2 symmetry was applicable and could contribute to better define our 3D models. The final resolution was 4.7 Å.

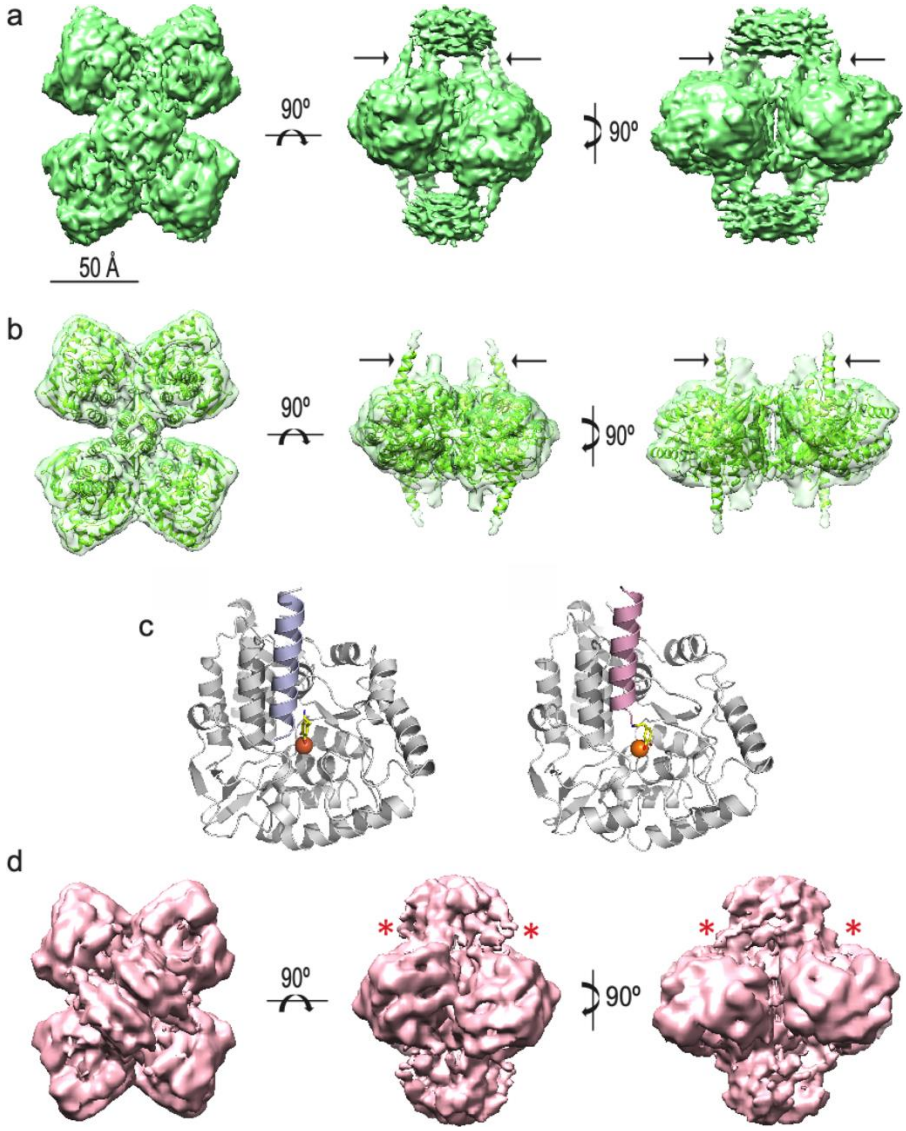

3d reconstruction of THNΔ35(DA). A) Three orthogonal views of the three-dimensional reconstruction of THNΔ35 in the presence of DA (THNΔ35(DA)). The black arrows point to a new mass visualized in TH(DA), which is not present in apo-TH. B) The same views with the atomic model of CD + OD domains of THNΔ35 (the RDs have been removed) docked into the corresponding mass of the THNΔ35 three-dimensional reconstruction. The black arrows point to the α-helix entering into the active site. C) Comparison of the atomic model of the TH active site of TH(DA) (left) and THNΔ35(DA) (right) showing the similar location of the α-helix inside the active site. D) Three orthogonal views of the three-dimensional reconstruction of phosphorylated on S40 (THS40p). The asterisks point to the position where the N-terminal α-helix is located in both TH(DA) and THNΔ35(DA) reconstructions, but absent in this structure.

MX2443 - Structure of the DNAJA2 chaperonin arranged as a helical complex (José María Valpuesta)

Session	Date	Micrographs	Ptcls	Fractions	Å/px	Images/hole
MX2443	3-5/05/2023	10714		40	1.054	2

The structure obtained with the data acquired in these sessions were published in the reference:
Velasco-Carneros L, Cuéllar J, Dublang L, Santiago C, Maréchal JD, Martín-Benito J, Maestro M, Fernández-Higuero JA, Orozco N, Moro F, Valpuesta JM, Muga A. "The self-association equilibrium of class A J-domain proteins DNAJA2 regulates its interaction with unfolded substrate proteins and with Hsc70. 2023. Nat. Commun (in the press)
EMDB IDs: EMD-14729, EMD-14706, EMD-14727, EMD-14736.
PDB ID: 7ZHS

The DNAJA2wt cryoEM grids were checked, and data from the best one acquired in a 200 kV FEI Talos Arctica equipped with a Falcon III direct electron detector at the Centro Nacional de Biotecnología (CNB) cryoEM facility. A total of 1482 movies were acquired at a nominal magni fication of ×73000 (corresponding to a pixel size of 1.37 Å/pixel), with a defocus range of −1.2 to −3.4 µm. Movies were fractionated to 60 frames with an exposure time of 1 s and a dose rate of 61 e^-/pixel/s The total accumulated dose was 32 e − /Å2 (0.53 e − /Å 2 /frame). DNAJA2 ΔG/FR samples were first checked on a 200 kV FEI Talos Arctica at the CNB followed by data acquisition on a FEI Titan Krios electron microscope (Krios 1) operated at 300 kV, equipped with a Gatan Quantum K3 Summit direct electron detector mounted on a Gatan Bioquatum LS/ 967 energy filter at the European Synchrotron Radiation Facility (ESRF) in Grenoble. Data collection was carried out with a 130000x nominal magni fication (yielding a pixel size of 1.053 Å/pixel) and a defocus range of −1.2 to −2.6 µm. A total of 10714 movies were recorded and each movie was fractionated to 40 frames with an exposure time of 5 s and a dose rate of 8.15 e − /pixel/s. The total accumulated electron dose was 36 $e^-/Å^2$ (0.90 $e^-/Å^2$ /frame). The representative cryoEM images shown in this study were observed in independent experiments with three different protein preparations

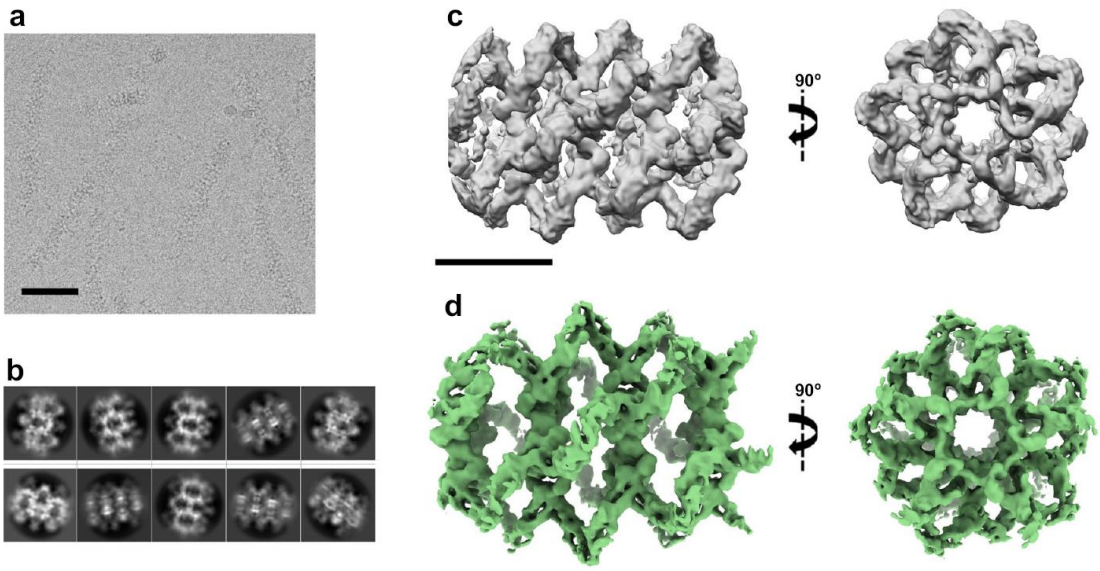

CryoEMstructure ofDNAJA2ΔG/FR. A) AcryoEMfield ofDNAJA2ΔG/FR. Bar indicates 500 Å. B) Maximum-likelihood 2D classification of the collected particles. C) Side and top views of the 3D reconstruction of DNAJA2ΔG/FR without symmetry imposition. D) Side and top views of the D5-symmetry imposed DNAJA2ΔG/FR map (6.9 Å resolution). Bar in (c) and (d) indicates 100 Å.

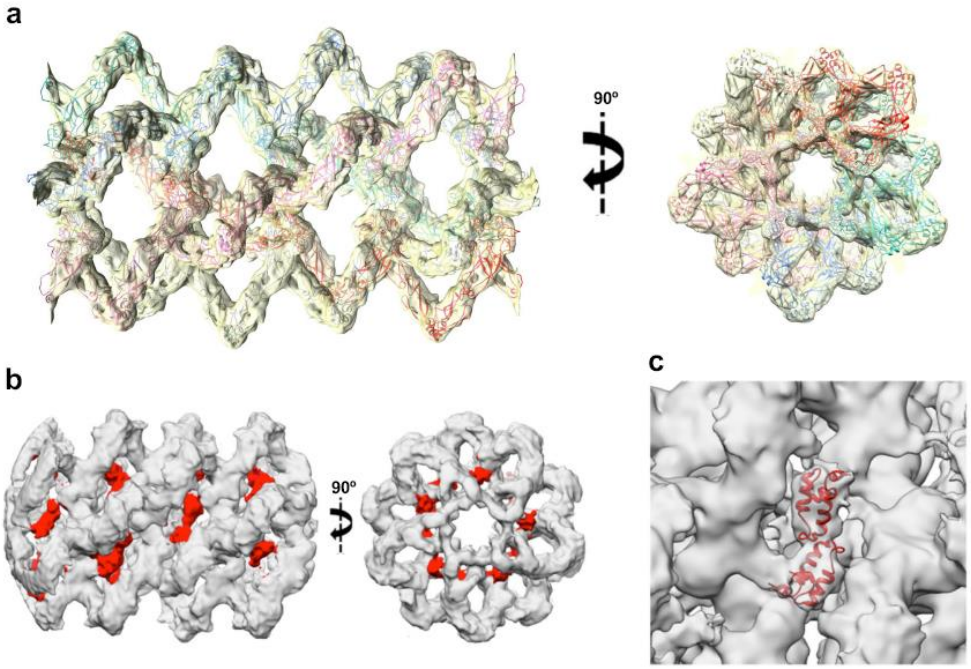

Atomic model of DNAJA2ΔG/FR in the helicoidal arrangement. A) Side and top views of the atomic model of DNAJA2ΔG/FR fitted into the 3D reconstruction shown in Fig. 2d. Each filament that forms the oligomer is coloured differently. B) Side and top views of the 3D reconstruction of DNAJA2ΔG/FR without symmetry imposition, highlighting the position of the JDs (in red). C) Detail of two JDs of adjacent DNAJA2 monomers docked into the C1 DNAJA2ΔG/FR 3D reconstruction.

MX2443 – Structure of Human α2-macroglobulin (hα2M) (Daniel Luque)

Session	Date	Micrographs	Ptcls	Fractions	Å/px	Images/hole
MX2443	7-9/10/2022	12143			1.047	

The structures obtained with the data acquired in these sessions were published in the reference:

Luque D, Goulas T, Mata CP, Mendes SR, Gomis-Rüth FX, Castón JR. Cryo-EM structures shows mechanisitics basis of pan-peptidase inhibition by human α2-macroglobulin. Proc Natl Acad Sci U S A. 2022 May 10;119(19):e2200102119. doi: 10.1073/pnas.2200102119. Epub 2022 May 2. PMID: 35500114.

EMDB IDs: EMD-12747, EMD-12748, EMD-12750, EMD-12751, EMD-12752, EMD-12753, EMD-12754, EMD-12755, EMD-12941, EMD-12942, EMD-12943, EMD-12944.

PDB IDs: 7O7L, 7O7M, 7O7N, 7O7O, 7O7P, 7O7Q, 7O7R, 7O7S, 6TAV, 4ACQ

Human α2-macroglobulin (hα2M) is an ~720-kDa homotetrameric particle with pan-peptidase inhibitory functions that transits between an open native conformation and a closed induced state, in which endopeptidases are trapped upon cleavage of an accessible bait region. We determined the molecular mechanism of this function through cryo-EM structures, which revealed that the hα2M subunits are organized in two flexible modules that undergo independent expanded-to-compact transitions.

Sample preparation and data acquisition.

Wild-type authentic native (hα2M)4 was isolated from thawed frozen plasma from healthy human donors, which was de-identified prior to use in this study. The protein was purified, assessed for peptidase-inhibition competence as described (15, 26, 49), and verified to be equivalent to protein purified from fresh plasma in functional and physiological assays. Aliquots of pure protein (5 µL) were diluted to 0.1 mg/mL, applied to R2/2 300 mesh acetone vapor-treated copper grids, and vitrified using a Leica EM CPC cryofixation unit. Data were collected on FEI Titan Krios electron microscopes operated at 300 kV, and images were recorded with Gatan K3-summit cameras in counting mode using the EPU Automated Data Acquisition Software for Single Particle Analysis (Thermo Fisher Scientific).

Image Processing.

Movies were drift-corrected and dose-weighted with Motioncor2, and contrast transfer function values were estimated with CTFFIND4.1. All subsequent image processing was with RELION 2.1, unless otherwise stated. The data processing workflows for (hα2M)4 complexes purified from plasma are described in figure 1. Class averages from preliminary datasets were used as templates for subsequent automated particle picking with Gautomatch. Particles were then subjected to several rounds of reference-free 2D classification to discard particles that did not show secondary structural elements. Selected particles were 3D classified, imposing C2 symmetry for plasma-purified (hα2M)4 complexes. Classes representing equivalent conformational states were pooled and included in a 3D auto-refinement. Particles assigned to a native state were submitted to an additional round of 3D classification without alignment to identify and refine particles corresponding to native I and II states. To identify and classify intermediate conformations between the (hα2M)4 major states in plasma, the C2 symmetry of these states was expanded and particles were subjected to 3D classification without alignment. Classes representing equivalent conformational states were pooled and included in a 3D auto-refinement. Local resolution was estimated using MonoRes (figure 2) and unsharpened maps treated by local resolution-based sharpening in LocalDeblur.

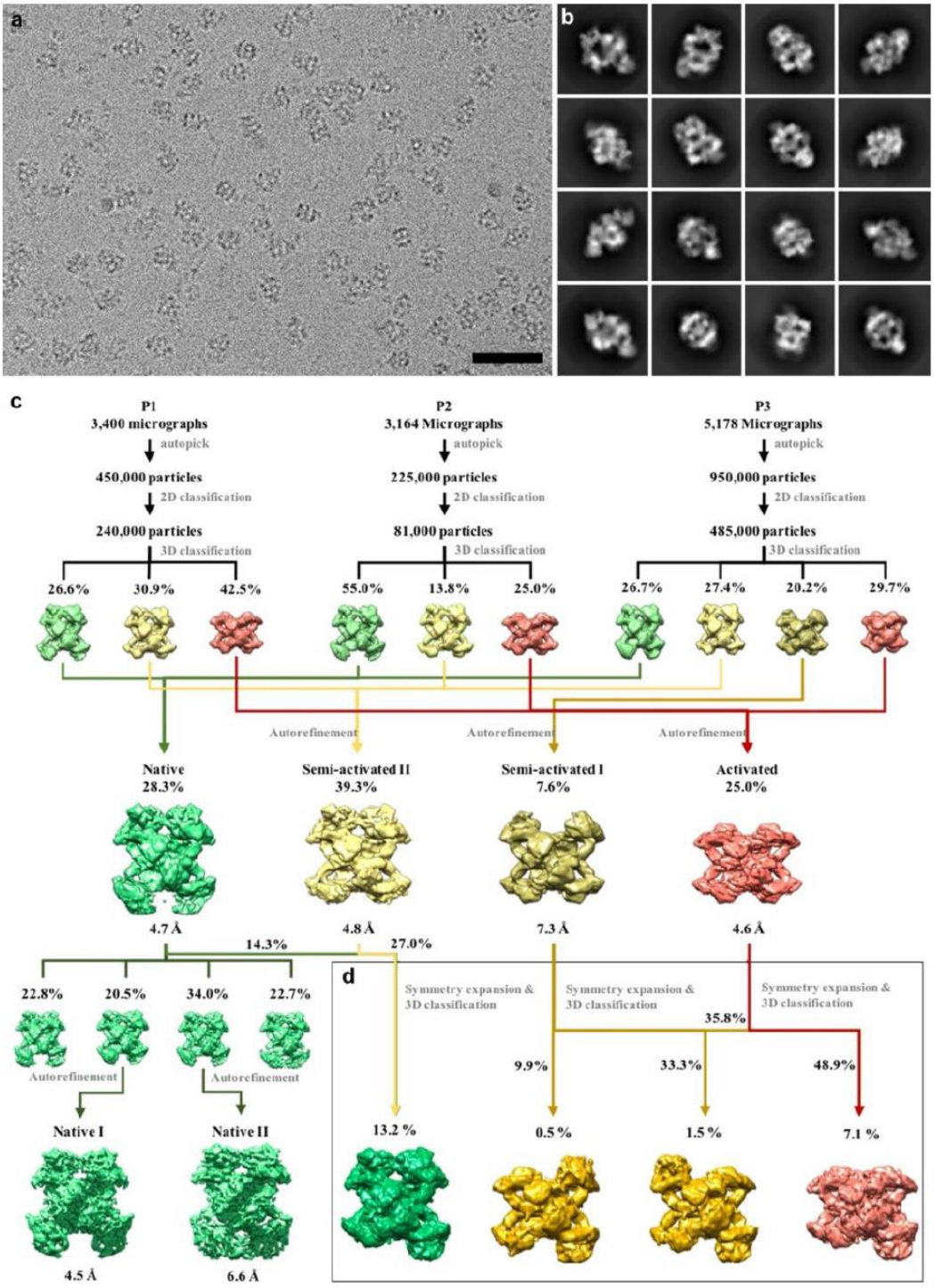

Figure 1. Cryo-EM data processing of (hα2M)4 corresponding to the native untreated fraction. (a) Representative cryo-EM image of (hα2M)4 complexes (bar, 500 Å). (b) 2D class averages of (hα2M)4. (c) Data processing workflow and structure determination of the five functional states of (hα2M)4 using three serum preparations (P1-P3). After 3D classification, three (green, yellow, and red for preparations P1 and P2) and four (green, yellow, gold, and red for P3) distinct conformational states were identified (percentages indicated relative to total 3D selected particles of each preparation). Particles of each of the four states were combined into four separate datasets and further refined. The global resolution of each of the resulting 3D reconstructions was 4.7, 4.8, 7.3 and 4.6 Å, respectively, and the percentages relative to the sum of particles in the four classes was 28, 39, 8, and 25%, respectively. The dataset corresponding to truly native (hα2M)4 (green) was further classified and two conformational

states were refined, yielding resolutions of 4.5 and 6.6 Å for native I and II states, respectively. (d) The C2 symmetry of the native, semi-activated I plus II and activated states was expanded and the particles from each state were subjected to additional 3D classification without alignment. Classes representing equivalent conformational states (percentages relative to the parental state are indicated) were pooled, resulting in 3D reconstructions of four new intermediate transient states.

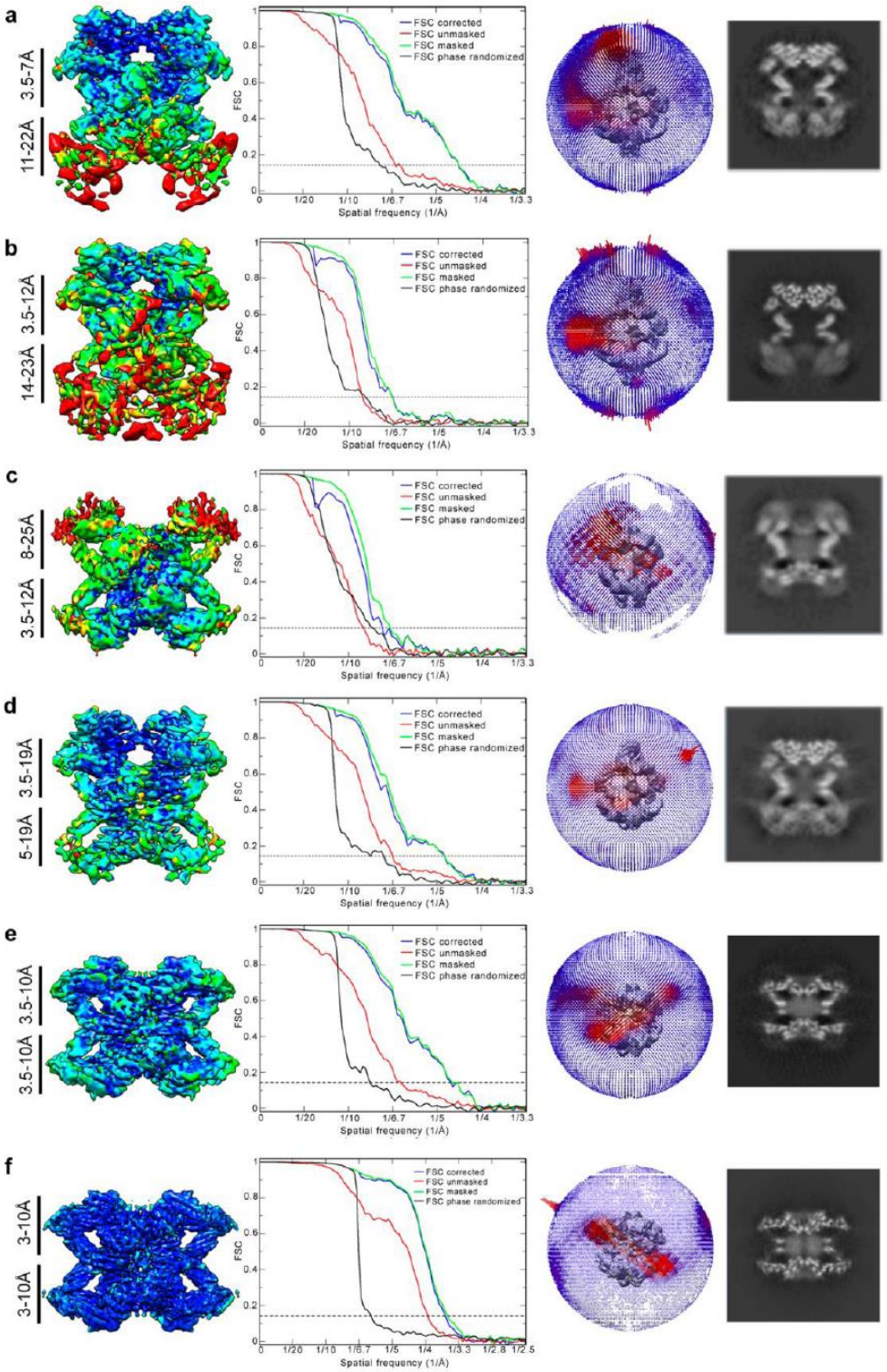

Figure 2: Global and local resolution of cryo-EM maps. Local resolution assessment and Fourier shell correlation (FSC) curves for the eight maps calculated in this study: (a) native I, (b) native II, (c) semi-activated I, (d) semi-activated II, (e) fully activated state,

MX2443 – Structure of Vault ribonucleoprotein (Nuria Verdaguer)

Session	Date	Micrographs	Ptcls	Fractions	Å/px	Images/hole
MX2443		3407			1.047	

The structures obtained with the data acquired in these sessions were published in the reference:
Guerra P, González-Alamos M, Llauró A, Casañas A, Querol-Audí J, de Pablo PJ, Verdaguer N. Symmetry disruption commits vault particles to disassembly. Sci Adv. 2022 Feb 11;8(6):eabj7795. doi: 10.1126/sciadv.abj7795. Epub 2022 Feb 9. PMID: 35138889.
EMDB IDs: EMD-13478, EMD-13483, EMD-13482.
PDB IDs: 7PKR.

Vaults are ubiquitous ribonucleoprotein particles involved in a diversity of cellular processes, with promising applications as nanodevices for delivery of multiple cargos. The vault shell is assembled by the symmetrical association of multiple copies of the major vault protein that, initially, generates half vaults. The pairwise, anti-parallel association of two half vaults produces whole vaults. Here, using a combination of vault recombinant reconstitution and structural techniques, we characterized the molecular determinants for the vault opening process.

Cryo-EM and data acquisition.

For cryo-EM, an aliquot of 3 µl of recombinant vault sample was applied during 15 s to each EM grid with holey gold film. After that, the grid was blotted with Vitrobot (FEI, Eindhoven, The Netherlands) in 100% humidity for 3 s and then plunged into liquid ethane to vitrify the sample. Movies were obtained in Titan Krios 300-kV EM (FEI, Eindhoven, The Netherlands) equipped with a Gatan K3 direct electron detection camera at ×81,000. The pixel size was measured to 1.78 Å on the specimen scale. We used an electron dose rate of 8 electrons per pixel per second, and each movie contains 30 frames recorded in 12 s. Image stacks in each movie were aligned with MotionCor2 (28). The 30 frames in each stack were averaged to obtain a dose weight of 30 e^{-}/ A^2. The whole dataset has 3407 movies. A second dataset was collected at pixel size 1.07 Å per pixel, corresponding to a magnification of ×130,000. We used an electron dose rate of 7.4 electrons per pixel per second, and each movie contains 40 frames recorded in 8 s.

Image processing and 3D reconstruction

Aligned micrographs were used for the contrast transfer function (CTF) estimation using Gctf, with defocus values ranging from −1.5 to −3.5 µm. A total of 34,822 particles were automatically picked using RELION with a box of 400 × 400 pixels of size. All picked particles were classified using RELION. The classes with no interpretable features were discarded. A total of 9793 particles were selected for 3D classifications to calculate the

closed vault map and 7539 particles were selected to calculate the half vault map. The initial model for Class3D was generated from a previous atomic model (PDB: 4HL8) of rat vault low-filtered to 60 Å resolution to eliminate the risk of model bias. In the closed vault reconstruction, particles were subjected to consecutive Class3D and Refine3D jobs and additionally to CTF refinement and particle polishing. This class was refined separately with RELION by applying D39 symmetry. To enhance the signal, a mask was generated around the whole vault, obtaining a map after RELION postprocessing of 3.7 Å. The resolution was determined based on a "gold standard" FSC coefficient of 0.143.

A model of the vault particle (PDB ID: 4HL8) was docked into the map using UCSF Chimera, and Coot was used to manually adjust these initial models. An initial round of refinement was performed in Phenix using real-space refinement.

In the case of the half vault, Class3D analysis allowed to calculate a map that presented a reasonable resolution (around 14 Å). This half vault class was refined separately with RELION by applying C1 symmetry. To enhance the signal, a mask was generated around the whole half vault, obtaining a map after RELION postprocessing of 9.3 Å. The resolution was determined based on a gold standard FSC coefficient of 0.143.

The vault in committed conformation was obtained by the data analysis of the second dataset. A total of 207,815 particles were automatically picked using RELION (21) with a 700 × 700 pixels box. All picked particles were classified using RELION in a 2D classification process (Class2D). A total of 11,666 particles were selected for further 3D classifications (Class3D) that yielded the vault reconstruction in committed conformation. This class was refined separately without imposing any symmetrical condition, obtaining a map of 7.9 Å. The resolution was determined based on a gold standard FSC coefficient of 0.143.

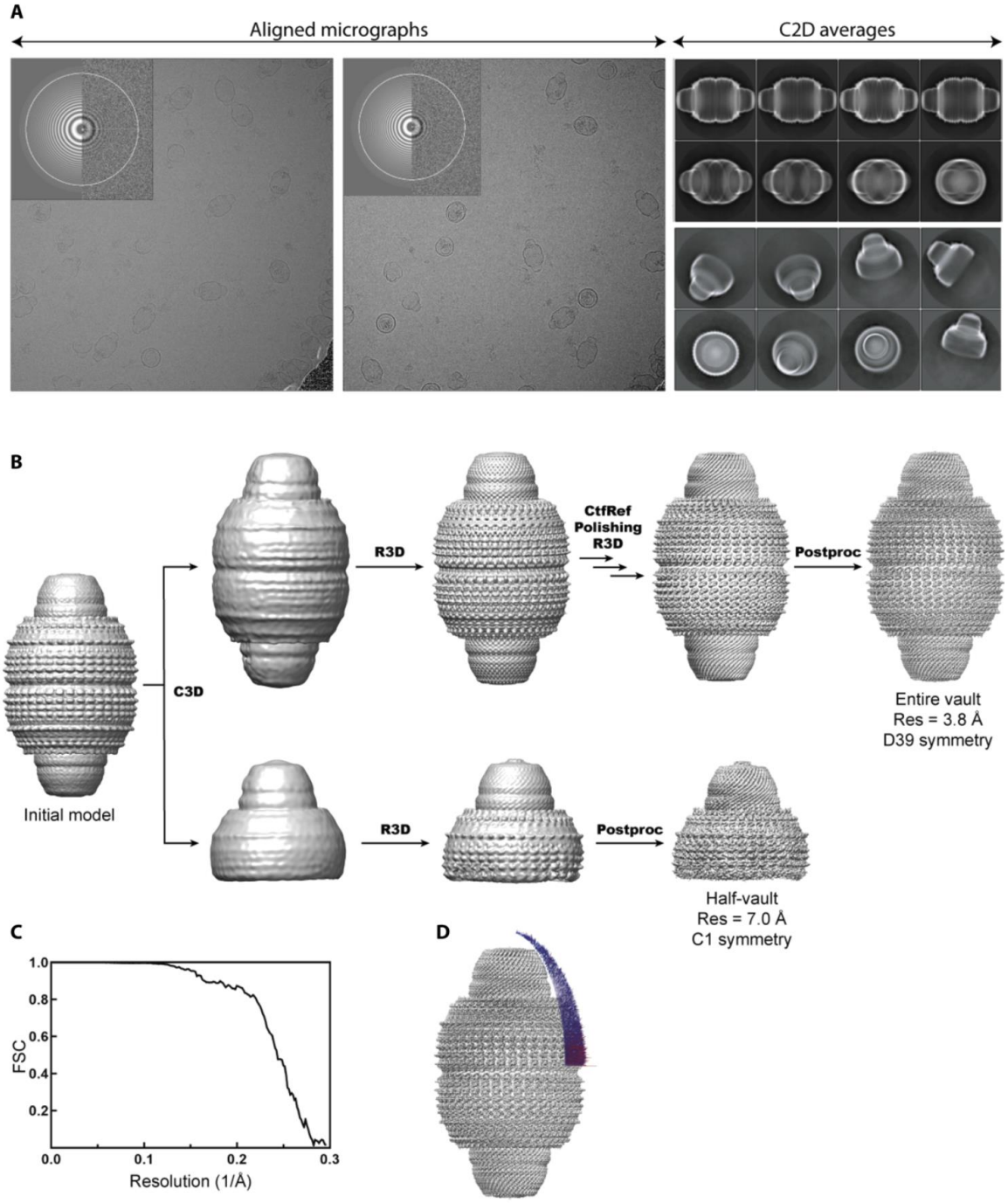

Cryo-EM representative images, classification workflow, FSC correlation curve and angular distribution for the symmetrical vault class. (A) Left, two representative aligned micrographs. Right, representative reference-free two-dimensional class averages (B) Image processing workflow used to characterize the heterogenous dataset what allowed the identification of several populations. (C) Gold-standard Fourier Shell Correlation (FSC) curves between half maps refined independently using Relion 3. Global resolution by the 0.143 cutoff criterium was estimated to be 3.7 Å. (D) Angular distribution of vault particles that contributed to the final map.

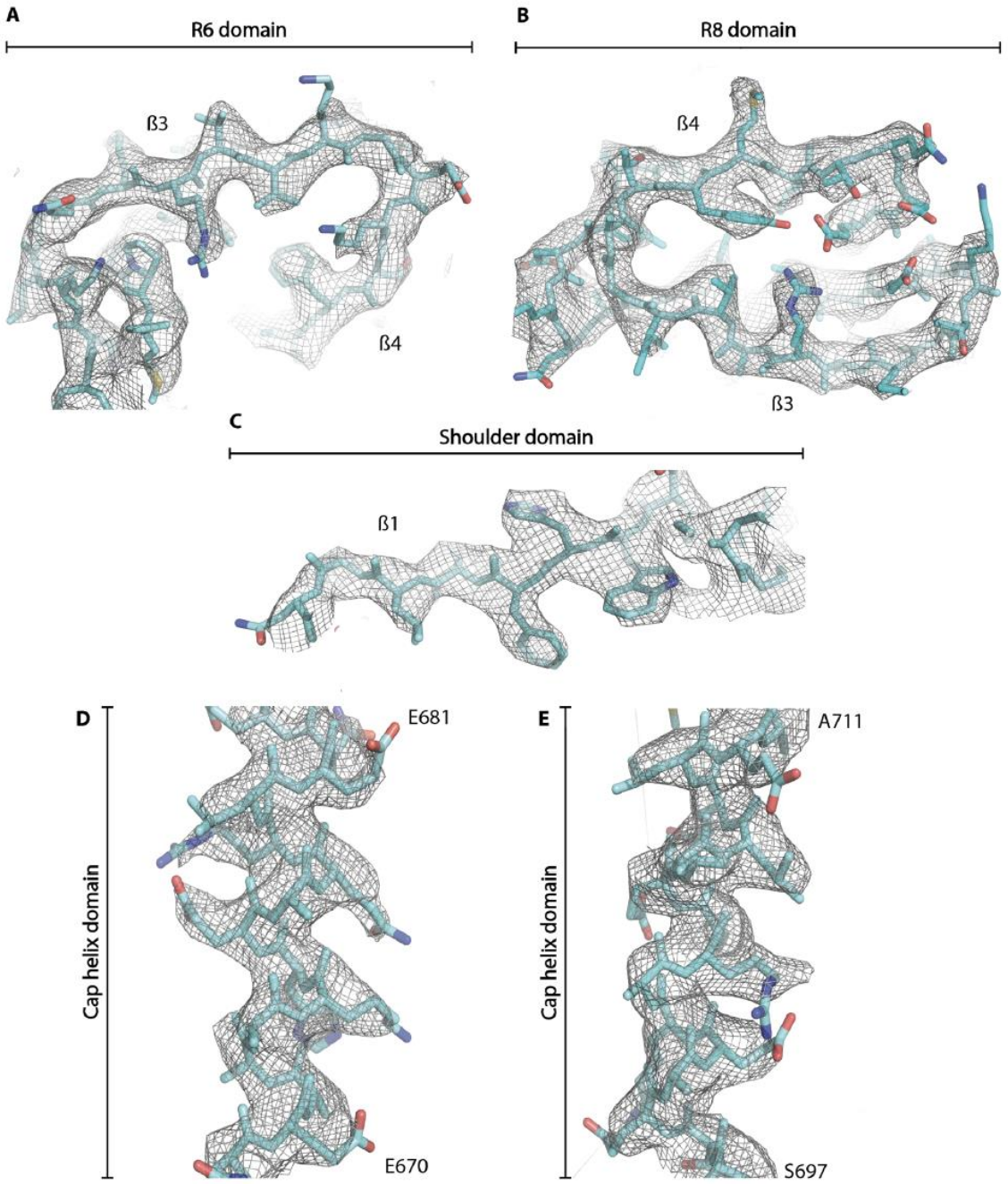

Figure S2. Experimental cryo-EM density for selected regions of the symmetrical vault reconstruction. (A) Experimental cryo-EM density observed for the ß3 motif of the R6 domain. (B) Cryo-EM density observed for the ß3 and ß4 motifs of the R8 domain. (C) Cryo-EM density observed for the ß1 motif of the shoulder domain. (D and E) Cryo-EM density observed in the cap helix domain.